# Dynamic, M2-Like Remodeling Phenotypes of CD11c+ Adipose Tissue Macrophages During High-Fat Diet–Induced Obesity in Mice

**Merav E. Shaul, Grace Bennett, Katherine J. Strissel, Andrew S. Greenberg, and Martin S. Obin**

**OBJECTIVE**—To identify, localize, and determine M1/M2 polarization of epididymal adipose tissue (eAT) macrophages (Φs) during high-fat diet (HFD)-induced obesity.

**RESEARCH DESIGN AND METHODS**—Male C57BL/6 mice were fed an HFD (60% fat kcal) or low-fat diet (LFD) (10% fat kcal) for 8 or 12 weeks. eATMΦs (F4/80$^+$ cells) were characterized by in vivo fluorescent labeling, immunohistochemistry, fluorescence-activated cell sorting, and quantitative PCR.

**RESULTS**—Recruited interstitial macrophage galactose-type C-type lectin (MGL)1$^+$/CD11c$^-$ and crown-like structure–associated MGL1$^-$/CD11c$^+$ and MGL1$^{med}$/CD11c$^+$ eATMΦs were identified after 8 weeks of HFD. MGL1$^{med}$/CD11c$^+$ cells comprised ~65% of CD11c$^+$ eATMΦs. CD11c$^+$ eATMΦs expressed a mixed M1/M2 profile, with some M1 transcripts upregulated (IL-12p40 and IL-1β), others downregulated (iNOS, caspase-1, MCP-1, and CD86), and multiple M2 and matrix remodeling transcripts upregulated (arginase-1, IL-1Ra, MMP-12, ADAM8, VEGF, and Clec-7a). At HFD week 12, each eATMΦ subtype displayed an enhanced M2 phenotype as compared with HFD week 8. CD11c$^+$ subtypes downregulated IL-1β and genes mediating antigen presentation (I-a, CD80) and upregulated the M2 hallmark Ym-1 and genes promoting oxidative metabolism (PGC-1α) and adipogenesis (MMP-2). MGL1$^{med}$/CD11c$^+$ eATMΦs upregulated additional M2 genes (IL-13, SPHK1, CD163, LYVE-1, and PPAR-α). MGL1$^{med}$/CD11c$^+$ ATMΦs expressing elevated PGC-1α, PPAR-α, and Ym-1 transcripts were selectively enriched in eAT of obese mice fed pioglitazone for 6 days, confirming the M2 features of the MGL1$^{med}$/CD11c$^+$ eATMΦ transcriptional profile and implicating PPAR activation in its elicitation.

**CONCLUSIONS**—These results *1*) redefine the phenotypic potential of CD11c$^+$ eATMΦs and *2*) suggest previously unappreciated phenotypic and functional commonality between murine and human ATMΦs in the development of obesity and its complications. ***Diabetes*** **59:1171–1181, 2010**

From the Obesity and Metabolism Laboratory, Jean Mayer U.S. Department of Agriculture Human Nutrition Research Center on Aging, Tufts University, Boston, Massachusetts.

Corresponding authors: Martin S. Obin, martin.obin@tufts.edu, or Andrew S. Greenberg, andrew.greenberg@tufts.edu.

Received 21 September 2009 and accepted 14 February 2010. Published ahead of print at http://diabetes.diabetesjournals.org on 25 February 2010. DOI: 10.2337/db09-1402.



Chronic inflammation is a pathogenic factor in obesity complications, in particular insulin resistance (1,2). A significant advance in our understanding of obesity-associated inflammation and insulin resistance has been recognition of the underlying role of adipose tissue macrophages (ATMΦs) (1–4). Tissue MΦs are phenotypically heterogeneous and are broadly characterized according to activation (polarization) state by the M1/M2 classification system (5,6): Classical M1 activation induced by interferon-γ and lipopolysaccharide (LPS) defines proinflammatory, microbicidal MΦs. M1 MΦs are the first line of defense against intracellular pathogens, and they prime toward a Th1 adaptive immune response by producing interleukin (IL)-12 (7). In contrast, MΦs expressing one of several overlapping M2 polarization states are activated by IL-4/IL-13 (M2a or "alternative" activation), diverse stimuli (e.g., apoptotic cells) in concert with LPS (M2b), or IL-10, transforming growth factor (TGF)-β, or glucocorticoids (M2c). M2-polarized MΦ function in tissue remodeling during development and in response to injury, and they promote the resolution of acute inflammation. Although M2a polarized MΦs are also involved in antiparasite defense and Th2 priming, it has been suggested that the predominant role of M2-polarized MΦs is the regulation of tissue homeostasis (8,9). Thus, M2-polarized MΦs typically upregulate arginase (ARG)-1 and downregulate inducible nitric oxide sythase (iNOS) (thereby promoting collagen production at the expense of microbicidal NO); elevate the expression of inflammation-suppressive factors (IL-10 and IL-1Ra), matrix metalloproteinases (MMPs), and proangiogenic mediators; and express an overall attenuated proinflammatory and Th1-priming gene expression profile.

Our current understanding of how ATMΦs promote obesity-associated inflammation and insulin resistance is based in large part on the "phenotype switch" model of Lumeng et al. (10). In this model, obesity promotes the recruitment of M1-polarized ATMΦs that shift the noninflammatory milieu maintained by M2a polarized, resident ATMΦs toward a proinflammatory state. In epididymal AT (eAT), these M1 ATMΦs (eATMΦs) are distinguished by *1*) localization to crown-like structures (CLS) and cell "clusters" of active remodeling around dead adipocytes (7,11,12), *2*) elevated expression of the CC chemokine receptor CCR2 and the dendritic cell marker CD11c in conjunction with downregulation of the signature M2 lectin macrophage galactose-type C-type lectin (MGL)1 (11), and *3*) by an M1 gene expression profile featuring upregulated iNOS and downregulated ARG-1 (10,11,13).

The M1 polarization of eATMΦs is in certain respects counterintuitive. Adipose tissue expansion is a process of

coordinated tissue remodeling and repair involving removal of apoptotic cells (adipocytes), extracellular matrix remodeling, angiogenesis, and new adipogenesis (12,14–16). In other tissues, these types of remodeling and reparative processes typically involve M2-polarized MΦs (5,6). Moreover, these features of adipose tissue remodeling are manifest in or near the "clusters" to which $CCR2^+$ and/or $CD11c^+$ eATMΦs selectively localize, and roles for cluster-associated eATMΦs in adipocyte clearance and angiogenesis have been proposed (7,12,14). In humans, fat mass expansion is associated with the accumulation of anti-inflammatory or mixed M1/M2-polarized ATMΦs (17). These ATMΦs exhibit "remodeling" phenotypes (18) characterized by increased MMP activities and elevated expression of lymphatic vessel endothelial hyaluronan receptor (LYVE)-1, a mediator of adipose tissue angiogenesis (19). Considered together, these observations suggest that one or more populations of recruited eATMΦs are likely to express features of an M2-like remodeling phenotype during the development of murine obesity and insulin resistance.

Here we identify, localize, and transcriptionally characterize eATMΦ subtypes in mice fed a high-fat diet (HFD) for 8 or 12 weeks, a period of progressively increasing body weight, eAT remodeling, eATMΦ recruitment, and whole-body insulin resistance (12). Our observations redefine the phenotypic potential of $CD11c^+$ eATMΦs and suggest that obesity and insulin resistance develop in this model in association with a coincident M2 and M1 phenotypic progression.

## RESEARCH DESIGN AND METHODS

**Animals and diets.** Six-week-old male C57BL/6j mice were fed a low-fat diet (LFD) (10% energy from fat) or an HFD (60% energy from fat) (12) for 8, 10, or 12 weeks at The Jackson Laboratory (Bar Harbor, ME). Following overnight shipment, mice were fed the same diets in a viral pathogen–free facility for 2–3 days before use. Mice fed an HFD for 10 weeks were maintained for an additional 6 days at the Human Nutrition Research Center on Aging on either an HFD or an HFD containing (0.01%, wt/wt) pioglitazone (PIO) (HFD+PIO). Six-week-old standard diet–fed mice were maintained for an additional 4 weeks on standard diet or HFD following in vivo phagocyte labeling with PKH26 (see below). Mice were killed by $CO_2$/cervical dislocation, and eAT was processed as described below. All procedures adhered to Human Nutrition Research Center on Aging Institutional Animal Care and Use Committee Guidelines.

**Intraperitoneal insulin tolerance test (ITT).** Whole-body insulin resistance was determined in mice as described (12).

**Immunohistochemistry and immunofluorescence.** Paraffin sections were probed with goat anti-mouse MGL1 (R&D Systems, Minneapolis, MN) or with IgG isotype control followed by horseradish peroxidase–conjugated second antibody (12). For immunofluorescence, eAT was fixed in zinc-paraformaldehyde (Zn-PFA) (20), minced into ~1 × 1 × 1 mm pieces, blocked with horse serum, and incubated with MGL1 antibody in PBS/horse serum (o/n, 4°C) followed by DyLight488-conjugated secondary antibody and Hoechst reagent.

**Stromal vascular cell isolation.** eAT was placed into Krebs-Henseleit buffer (21) supplemented with 4% fatty acid–free BSA, 5 mmol/l D-glucose, and 200 nmol/l PIA; minced; centrifuged (500*g*, 5 min, room temperature); digested (30–40 min, 37°C) with endotoxin-free Liberase 3 (0.3 units/ml, Roche Applied Science, Indianapolis, IN) containing 50 units of DNase I (Sigma-Aldrich); passed through a sterile 100-μm strainer (Fischer Scientific, Franklin, MA); and centrifuged (500*g*, 5 min, room temperature). Following incubation with erythrocyte lysis buffer, stromal vascular cells (SVCs) were resuspended ($1 \times 10^6$ cells/100 μl) in cold fluorescence-activated cell sorting (FACS) buffer (PBS containing 1 mmol/l EDTA, 25 mmol/l HEPES, and 1% [wt/vol] fatty acid–free BSA) until immunolabeling.

**Flow cytometry and SVC sorting.** SVCs were incubated on ice (10 min) with FcBlock (5 μg/ml) (BD Pharmingen, San Jose, CA), followed by incubation with fluorophore-conjugated antibodies or isotype controls. Antibodies included phycoerythrin-Cy5–conjugated F4/80 (eBioscience, San Diego, CA), phycoerythrin-conjugated CD11c (BD Pharmingen, Franklin Lakes, NJ), goat anti-mouse MGL1 (R&D Systems), and donkey anti-goat DyLight488 (Jackson ImmunoResearch Laboratories, West Grove, PA). Cells were analyzed using a FACScalibur flow cytometer equipped with CellQuest software (Becton Dickinson, San Jose, CA) or sorted on a MoFlo multilaser system sorter (Beckman Coulter, Brea, CA) using Summit software (Beckman Coulter). Gating and compensation strategies are depicted in Fig. 1 and supplemental Fig. 1 (available at http://diabetes.diabetesjournals.org/cgi/content/full/db09-1402/DC1). Sorted ATMΦs were collected in buffer containing RNase inhibitor and stored at −70°C.

**PKH26 labeling of adipose tissue phagocytes.** Six-week-old standard diet–fed mice were injected (intraperitoneally) with 200 μl of 0.5 μmol/l PKH26 (Sigma-Aldrich, St. Louis, MO). Four days later, mice were assigned to either standard diet or HFD cohorts for 4 weeks, after which ATMΦs in eAT were analyzed by FACS.

**Quantitative PCR.** RNA was extracted using RNeasy Mini and RNeasy MinElute Cleanup kits (Qiagen) and reverse transcribed and amplified using the WT-Ovation RNA Amplification System (NuGEN Technologies, San Carlos, CA). Quantitative PCR was conducted using SYBR Green (Applied Biosystems) (12). Fold differences in gene expression were calculated as $2^{-\Delta\Delta Ct}$ using cyclophilin A as the housekeeping gene. Primer sequences are in supplemental Table 1.

**Statistics.** Data are expressed as means ± SE. Means were compared by *t* test or by ANOVA or GLM procedures in conjunction with Tukey honestly significant difference test (SAS version 9.1). Significance was set at $P \leq 0.05$.

## RESULTS

**$CD11c^+$ ATMΦs with differential MGL1 expression levels are recruited to and accumulate in eAT of mice fed an HFD.** As reported (12) feeding the HFD for 8 weeks increased body and eAT weights and induced whole-body insulin resistance (Table 1). Although total SVCs increased in response to HFD, SVCs per gram eAT did not (Table 1). Flow cytometry (Fig. 1*A*) confirmed that the preponderance (>90%) of eATMΦs ($F4/80^+$ cells) in mice fed a LFD did not express CD11c and that the HFD induced the accumulation of $CD11c^+$ eATMΦs (10). Overall, there appeared to be a continuum of MGL1 expression rather than distinct populations of MGL1-expressing cells (Fig. 1*A* and *C*). When gated for MGL1, $CD11c^+$ eATMΦs unexpectedly exhibited a broad distribution of MGL1 staining intensity that partially overlapped that of $MGL1^+/CD11c^-$ cells (Fig. 1*A*, *bottom panel*). The overlapping and nonoverlapping cells were defined as $MGL1^{med}/CD11c^+$ and $MGL1^-/CD11c^+$, respectively, based on staining intensity (Fig. 1*A* and 1*B*) and transcript levels (Fig. 1*C* and supplemental Table 2). When only $CD11c^+$ cells were considered, cells designated as $MGL1^{med}/CD11c^+$ expressed three times the level of MGL1 mRNA than cells designated $MGL1^-/CD11c^+$ ($P = 0.001$). Surprisingly, $MGL1^{med}/CD11c^+$ eATMΦs comprised the majority of $CD11c^+$ cells (Fig. 1*D*). In vivo pulse experiments with the phagocyte-labeling dye PKH26 (Fig. 1*E*) suggest that similar to $MGL1^-/CD11c^+$ cells (Fig. 1*E* and 11), $MGL1^{med}/CD11c^+$ ATMΦs are recruited to eAT (i.e., are not derived from resident $MGL1^+/CD11c^-$ cells present at the initiation of HFD). PKH26 labeling (Fig. 1*E*) also revealed HFD-induced recruitment of new (PKH26-negative) $MGL1^+/CD11c^-$ eATMΦs.

$CD11c^+$ eATMΦs are the predominant component of CLS and cell clusters surrounding dead adipocytes (11). Immunofluorescent staining of whole eAT labeled numerous MGL1-expressing cells within such clusters (Fig. 2*A*, *bottom left panel*), consistent with the presence of $MGL1^{med}/CD11c^+$ eATMΦs (Fig. 1). As previously reported (11), some cell clusters were composed predominantly of $MGL1^-$ eATMΦs (Fig. 2*A*, *bottom right panel*). Immunohistochemistry revealed MGL1-expressing cells within CLS (Fig. 2*B*, *left panel*) and in areas of active remodeling around dead adipocytes (Fig. 2*B*, *right panel*). These results suggest that $MGL1^{med}/CD11c^+$ eATMΦs are

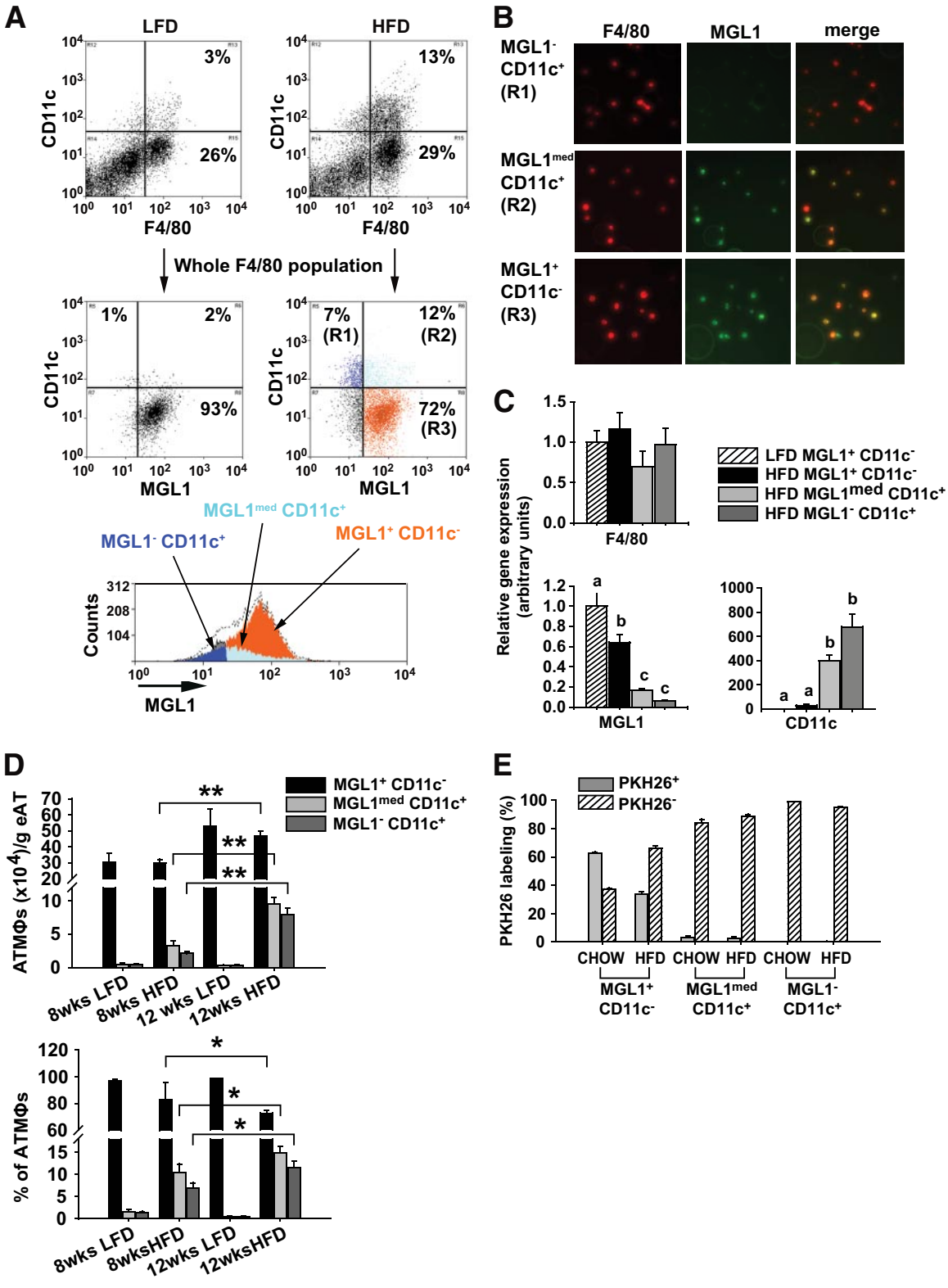


**FIG. 1. CD11c$^+$ eATMΦs exhibiting differential MGL1 expression (MGL1$^{med}$/CD11c$^+$ and MGL1$^-$/CD11c$^+$) accumulate in the eAT of mice fed an HFD. SVCs were obtained by collagenase digestion from eAT of mice fed an HFD or LFD for 8 weeks, labeled with F4/80, MGL1, and CD11c antibodies and analyzed by flow cytometry. *A*: HFD-associated increase in F4/80$^+$/CD11c$^+$ eATMΦs reflects increases in two ATMΦ subtypes, designated MGL1$^{med}$/CD11c$^+$ (R2) and MGL1$^-$/CD11c$^+$ (R1) according to their MGL1 staining intensity. *B*: Confirmation of MGL1 protein expression in MGL1$^+$/CD11c$^-$ and MGL1$^{med}$/CD11c$^+$ eATMΦs by fluorescence microscopy of sorted eATMΦs (as in *A*). *C*: Gene expression for F4/80, MGL1, and CD11c in sorted eATMΦ subtypes. *D*: Quantification of eATMΦ subtypes in response to 8 and 12 weeks of HFD demonstrating the absolute and proportional increase in CD11c$^-$ and CD11c$^+$ subtypes during the HFD time course. *P < 0.05; **P < 0.01, ANOVA and Tukey test. *E*: Evidence that MGL1$^{med}$/CD11c$^+$ eATMΦs are recruited rather than derived by phenotypic progression from resident MGL1$^+$/CD11c$^-$ cells. Lean mice were pulsed with the phagocyte-specific dye PKH26 and subsequently fed 2 standard diet or an HFD for 1 month followed by FACS of eATMΦs. Only ATMΦs present in eAT before clearance of the dye (24 h) express the label. (A high-quality digital representation of this figure is available in the online issue.)**

TABLE 1
Body and eAT weights, SVC numbers in eAT, and whole-body insulin resistance (ITT) in mice fed either the LFD or HFD for 8 ($n$ = 6) or 12 ($n$ = 7–11) weeks

| | Body weight (g) | eAT weight (g) | Total number of SVCs ($\times 10^6$) | Area under curve (ITT) |
|---|---|---|---|---|
| 8 weeks LFD | 28.27 ± 0.33* | 0.54 ± 0.02* | 1.23 ± 0.13* | 5,200 ± 260* |
| 8 weeks HFD | 37.65 ± 0.56† | 2.24 ± 0.19† | 4.78 ± 0.31† | 6,760 ± 315† |
| 12 weeks LFD | 29.21 ± 0.61* | 0.63 ± 0.06* | 1.99 ± 0.26* | — |
| 12 weeks HFD | 40.95 ± 0.61‡ | 1.86 ± 0.10† | 8.00 ± 0.71‡ | 7,890 ± 346‡ |

Data are means ± SE. Means identified by different symbols are significantly different ($P < 0.05$, ANOVA and Tukey procedure).

a significant component of some but not all cell clusters surrounding moribund adipocytes.

**eATMΦs express mixed M1/M2 transcriptional profiles after 8 weeks of HFD.** As expected, interstitial MGL1$^+$/CD11c$^-$ eATMΦs in mice fed an LFD displayed elevated levels of canonical M2 transcripts (IL-13, IL-10, Ym-1, sphingosine kinase 1 [SPHK1], signal transducer and activator of transcription [STAT]-6, CD206 [mannose receptor], and CD163 [hemoglobin scavenger receptor]) and relatively reduced levels of M1 transcripts (IL-12p40 and IL-1β) (Table 2; quantitative data summarized in Table 2 are presented in supplemental Fig. 2). In contrast, MGL1$^+$/CD11c$^-$ eATMΦs at HFD week 8 expressed elevated levels of CCR2 and several hallmark M1 transcripts (iNOS and IL-12p40), coincident with reduced expression of some M2 transcripts (IL-13, SPHK1, CD206, and CD163) and increases in M2 genes with inflammation-suppressive functions (IL-10, IL-1Ra, and STAT-6) (Table 2). These results indicate that the HFD recruits new interstitial MGL1$^+$/CD11c$^-$ eATMΦs (Fig. 1*E*) that express enhanced M1 and altered M2 transcriptional profiles.

Notably, neither CD11c$^+$ eATMΦ subtype expressed an overall M1-polarized phenotype after 8 weeks of HFD. Most surprisingly, ARG-1 expression was upregulated and iNOS expression was dramatically attenuated in CD11c$^+$ eATMs as compared with interstitial MGL1$^+$/CD11c$^-$ eATMΦs (Table 2). CD11c$^+$ eATMΦs also upregulated genes promoting tissue remodeling, including MMP-12 (22), and a proteinase with a disintegrin and metalloproteinase domain (ADAM)-8, a mediator of Th2-dependent airway remodeling in asthma (23). CD11c$^+$ eATMΦs also expressed relatively high levels of vascular endothelial growth factor (VEGF), and the MGL1$^-$/CD11c$^+$ subtype expressed more TGFβ-1 mRNA (Table 2). These remodeling signatures were associated with an M2-like expression pattern of several genes, including the upregulation of IL-1Ra interleukin-1 receptor antagonist and the downregulation of the M1-associated genes MCP-1 monocyte chemoatractant protein, caspase-1, and toll-like receptor (TLR)-4.

Both CD11c$^+$ subtypes also expressed relatively greater amounts of M1 transcripts with proinflammatory (IL-1β) and Th1-priming (IL-12p40) functions, and they downregulated several inflammation-suppressive (M2) genes (IL-10, IL-13, and STAT6) and the prototypic M2 markers Ym-1 CD206 and CD163 (Table 2). These data are consistent with the reported M1 polarization of MGL1$^-$ and CD11c$^+$ eATMΦs (10,11,24). However, expression of tumor necrosis factor-α and IL-6 were comparable in CD11c$^+$ and CD11c$^-$ eATMΦs (data not shown), perhaps reflecting the induction of these genes in CD11c$^-$ ATMΦs by the collagenase procedure (25). In summary, CD11c$^+$ eATMΦs in mice fed an HFD for 8 weeks express mixed M1 (proinflammatory) and M2 (remodeling) transcriptional profiles.

Levels of M1 and M2 transcripts in MGL1$^{med}$/CD11c$^+$ eATMΦs were intermediate between those measured in MGL1$^+$/CD11c$^-$ and MGL1$^-$/CD11c$^+$ eATMΦs, respectively (Table 2 and supplemental Fig. 2). When only gene expression data for HFD-fed mice were compared, transcript levels of 17 of 34 genes were significantly different in MGL1$^{med}$/CD11c$^+$ eATMΦs as compared with MGL1$^-$/CD11c$^+$ eATMΦs (supplemental Table 2). These observations support the viewpoint that MGL1$^{med}$/CD11c$^+$ eATMΦs are a distinct subtype with an intermediate phenotype consistent with the expression of both MGL1 and CD11c.

**Prolonged HFD feeding promotes distinctive patterns of altered gene expression in MGL1-expressing and CD11c-expressing eATMΦs.** As reported (12), 12 weeks of HFD induced weight gain, eAT remodeling (manifest as reduced eAT mass coincident with increased SVCs), and exacerbated whole-body insulin resistance (Table 1). Each of the three eATMΦ subtypes increased in number (per gram eAT) (Fig. 1*D*, *upper panel*), but the proportion of eATMΦs that were MGL1$^+$/CD11c$^-$ actually decreased (Fig. 1*D*, *bottom panel*). Of note, MGL1$^{med}$/CD11c$^+$ eATMΦs remained the predominant CD11c$^+$ eATMΦ subtype (Fig. 1*D*). At HFD week 12 eATMΦs exhibited global changes in the expression of genes involved in inflammation, antigen presentation, tissue remodeling, and metabolism consistent with increased M2 polarization, especially in the two MGL1-expressing subtypes (supplemental Fig. 3). The direction and magnitude of these changes are summarized in Fig. 3. MGL1$^+$/CD11c$^-$ and MGL1$^{med}$/CD11c$^+$ eATMΦs upregulated hallmark M2 genes (IL-13, Ym-1, SPHK1, and TGFβ-1), downregulated iNOS, and upregulated the adipogenic metalloproteinase MMP-2 (26) (Fig. 3). MGL1$^{med}$/CD11c$^+$ eATMΦs selectively upregulated LYVE-1 (19,27) while maintaining relatively high levels of VEGF and MMP-12 (Fig. 3). When compared with benchmark M2-polarized (MGL1$^+$/CD11c$^-$) eATMΦs from mice fed an LFD (Table 3), MGL1-expressing eATMΦs in mice fed an HFD for 12 weeks had comparable or a more pronounced M2-like expression profile of genes regulating inflammation, lipid metabolism, tissue remodeling, and antigen presentation. However, they continued to express M1-like levels of CD163, CD206, SPHK1 (reduced), and IL-12p40 (increased) as compared with M2-polarized eATMΦs from mice fed an LFD (Table 3).

Feeding the HFD for 12 weeks robustly upregulated the transcriptional coactivator peroxisome proliferator–activated receptor (PPAR)-γ coactivator (PGC)-1α in both CD11c$^+$ eATMΦ subtypes (Fig. 3), suggesting enhanced oxidative (i.e., M2-associated) metabolism (28). At this time, mRNA levels of both PGC-1α and PPAR-α (but neither PPAR-γ nor PPAR-δ) were three- to fivefold greater

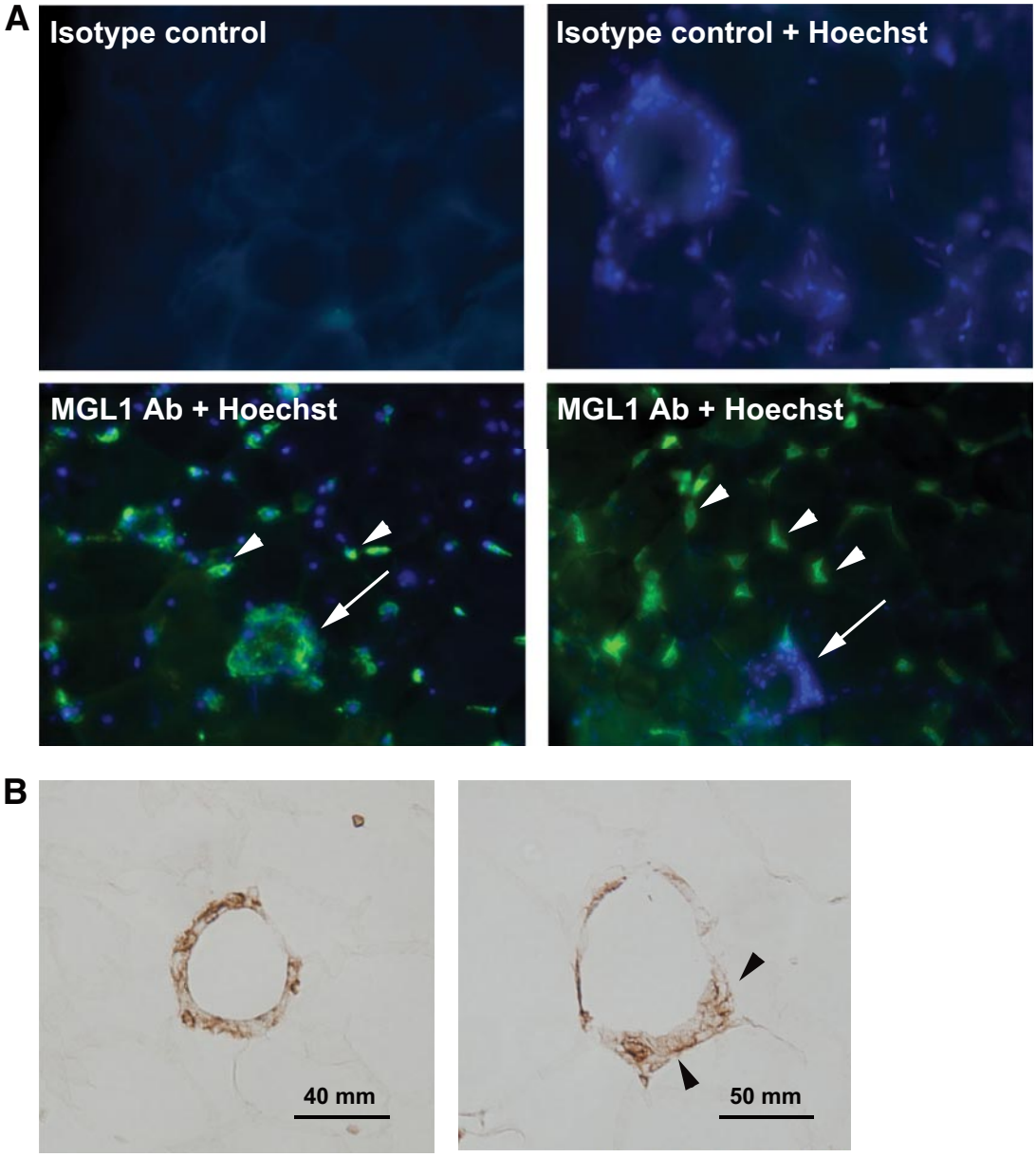


**FIG. 2. MGL1-expressing eATMs are associated with CLS and contiguous remodeling areas in eAT. *A*: MGL1 immunostaining was performed on eAT whole mounts from mice fed an HFD and examined by fluorescence microscopy. *Lower left panel*: MGL1-expressing cells (green) were localized to clusters (arrow) and interstitium (arrowheads). *Right lower panel*: An example of an MGL1-negative cluster. Blue color (Hoechst's reagent) identifies nuclei of MGL1$^-$ cells. *B*: MGL1 immunostaining of paraffin-embedded sections from mice fed an HFD. MGL1$^+$ cells are seen associated with MGL1$^-$ cells in CLS (*left panel*) and in associated remodeling areas (*right panel*, arrowheads). (A high-quality digital representation of this figure is available in the online issue.)**

in MGL1$^{med}$/CD11c$^+$ eATMΦs than in the other two eATMΦ subtypes ($P < 0.05$) (supplemental Fig. 4). CD11c$^+$ eATMΦs expressed relatively less IL-1β and genes involved in antigen presentation (I-a, CD80, and CD86) (Fig. 3). Overall, these results demonstrate M2-like changes in lipid/oxidative metabolism and inflammatory gene expression in CD11c$^+$ eATMΦs between weeks 8 and 12 of HFD. Importantly, when compared with benchmark M2-polarized eATMΦs (Table 3), CD11c$^+$ eATMΦs of mice fed an HFD for 12 weeks expressed comparable or greater levels of multiple M2-associated transcripts (STAT6, IL1-Ra, C type lectin [Clec]-7a, Arg-1, PGC-1α, TGFβ, MMP-2, MMP-12, VEGF, and ADAM-8) and equivalent or reduced levels of several M1-associated transcripts (iNOS, CD80, and CD86). These observations underscore the M2/remodeling features of the CD11c$^+$ eATMΦ transcriptional profile during HFD-induced obesity.

**MGL1$^{med}$/CD11c$^+$ ATMΦs preferentially accumulate in eAT of obese mice fed PIO.** As both PGC-1α and PPAR-α are targets of PPAR-γ, it was plausible that the M2-like gene expression changes observed in MGL1$^{med}$/CD11c$^+$ eATMΦs between weeks 8 and 12 of HFD (Fig. 3) reflected increased PPAR-γ activation (29). Accordingly, we phenotyped eATMΦs from mice maintained on HFD for 10 weeks and then fed either HFD or HFD containing the PPAR-γ/-α agonist PIO (HFD+PIO) for an additional 6 days. PIO treatment significantly ameliorated hyperinsulinemia and upregulated uncoupling protein-1 in eAT (Fig. 4), confirming PPAR-γ activation. Coincidentally, mRNA levels of both F4/80 and MGL1 were increased in mice fed

TABLE 2
Mixed M1/M2 remodeling transcriptional profiles in $CD11c^+$ eATMΦs at HFD week 8

| Gene | LFD $MGL1^+/CD11c^-$ | HFD $MGL1^+/CD11c^-$ | HFD $MGL1^{med}/CD11c^+$ | HFD $MGL1^-/CD11c^+$ |
|---|---|---|---|---|
| *M2* | | | | |
| ARG-1 | * | −* | ↑*† | ↑† |
| IL-1Ra | * | ↑† | ↑‡ | ↑‡ |
| TGFβ−1 | *† | ↓*† | ↓*† | ↑* |
| PGC-1β | * | ↑* | ↑* | ↑* |
| ADAM-8 | * | ↑† | ↑‡ | ↑§ |
| MMP-12 | * | ↑* | ↑† | ↑† |
| VEGF | * | ↑* | ↑† | ↑‡ |
| Clec7a | * | −* | ↑* | ↑* |
| IL-10 | *† | ↑* | ↓† | ↓‡ |
| IL-13 | * | ↓*† | ↓*† | ↓† |
| Ym-1 | * | −* | ↓* | ↓* |
| STAT-6 | * | ↑* | −* | −* |
| SPHK1 | * | ↓† | ↓† | ↓† |
| CD163 | * | ↓† | ↓‡ | ↓‡ |
| CD206 | * | ↓† | ↓‡ | ↓‡ |
| MMP-2 | * | ↓*† | ↓† | ↓† |
| *M1* | | | | |
| iNOS | *† | ↑† | ↓* | ↓* |
| IL-1β | * | −* | ↑† | ↑† |
| IL12p40 | * | ↑*† | ↑† | ↑† |
| I-a | *† | ↓* | ↑† | ↑‡ |
| CCR2 | * | ↑† | ↑†‡ | ↑‡ |
| MCP-1 | * | ↓† | ↓‡ | ↓‡ |
| Caspase-1 | *† | −* | ↓† | ↓*† |
| TLR4 | * | −* | ↓† | ↓† |
| CD86 | * | ↓† | ↓‡ | ↓‡ |
| CD80 | * | −* | −* | −* |
| STAT-1 | * | −* | −* | −* |

↓ and ↑ arrows indicate reduced or increased gene expression, respectively, as compared with $MGL1^+/CD11c^-$ eATMΦs from LFD-fed mice ($n = 6$) (see online appendix Fig. 2 for quantitative data summarized in this table). Transcript levels designated by different symbols are significantly different ($P < 0.05$, ANOVA and Tukey procedure).

HFD+PIO (Fig. 4), consistent with the recruitment of M2-polarized eATMΦs. Unexpectedly, CD11c mRNA levels also increased (Fig. 4). Flow cytometry revealed a selective increase in $MGL1^{med}/CD11c^+$ eATMΦs in mice fed HFD+PIO, resulting in a significant increase in the proportion of $CD11c^+$ cells expressing MGL1 (Fig. 4). These results suggest that $MGL1^{med}/CD11c^+$ ATMΦs are preferentially recruited and/or accumulate in eAT of HFD-fed mice in response to short-term systemic PPAR-γ agonism. Importantly, $MGL1^{med}/CD11c^+$ eATMΦs from mice fed HFD+PIO displayed elevated levels of Ym-1, PGC-1α, and PPAR-α (but not PPAR-γ) mRNAs (Fig. 4). This pattern of M2-associated gene expressions mirrors in part that observed in $MGL1^{med}/CD11c^+$ eATMΦs from mice fed HFD for 12 weeks (Fig. 3 and supplemental Fig. 4).

**Mixed M1/M2 remodeling transcriptional profile in whole eAT during HFD-induced obesity.** Finally, we determined a mixed M1/M2 and remodeling transcriptional profile at the tissue level during HFD-induced obesity. Quantitative PCR of selected eAT transcripts indicated that the expression of M2/remodeling genes MGL1, IL-10, IL-13, TGFβ-1, ADAM-8, and MMP-2 increased progressively in eAT during the course of HFD (Fig. 5). MMP12 mRNA (induced ≥300-fold in $CD11c^+$ eATMΦs) (Table 3) was upregulated ~100- and 150-fold in eAT at HFD weeks 8 and 12, respectively (data not shown). As expected, transcript levels of M1 cytokines (IL-12p40, IL-1β, and tumor necrosis factor-α) also increased during the HFD time course, but iNOS mRNA levels decreased at week 12 (Fig. 5), consistent with downregulation in eATMΦs (Table 3 and supplemental Fig. 3). Overall, these data demonstrate progressive, coordinate increases in the expression of both M2/remodeling and M1-associated genes in eAT during the course of HFD-induced obesity and insulin resistance (Table 1).

## DISCUSSION

Employing an established model of HFD-induced obesity (12), we demonstrate that eATMΦs recruited in response to HFD express mixed M1/M2 and remodeling transcriptional profiles and that these profiles become more M2-like with extended HFD feeding. Human ATMΦs have recently been shown to express mixed M1/M2 remodeling phenotypes (17,18), thus distinguishing them from the M1-polarized eATMΦs reported for obese mice (11,24). By demonstrating the pleiotropic transcriptional profiles of eATMΦs in murine obesity, the present study suggests previously unappreciated phenotypic and functional commonality between murine and human ATMΦs in the development of obesity and its complications.

We identified three subtypes of recruited eATMΦs in mice fed an HFD, including the $MGL1^+/CD11c^-$ and $MGL1^-/CD11c^+$ eATMΦs that were previously reported to be M2a and M1 polarized, respectively (11). In contrast to a recent report (30), our sorting strategy did not identify $CD11c^-$ and $CD11c^+$ eATMΦs as $F4/80^{lo}$ and $F4/80^{hi}$, respectively (Fig. 1*A* and *C*). As expected, interstitial $MGL1^+/CD11c^-$ eATMΦs were M2 polarized in mice fed an LFD (Table 2). HFD induced the recruitment of $MGL1^+/CD11c^-$ eATMΦs expressing an altered M2 transcriptional profile and elevated levels of several M1 transcripts (Table 2). These recruitment data, obtained in young, lean PKH26-injected mice subsequently fed an HFD differ from results of a prior study (11) that reported little or no recruitment of interstitial ($MGL1^+$) eATMΦs in older, obese HFD-fed mice injected with PKH26.

HFD did not elicit classical M1 polarization in $MGL1^-/CD11c^+$ eATMΦs but rather a mixed M1/M2-like pattern of gene expression characterized by enhanced expression of IL-12p40 and IL-1β (M1) coincident with downregulated expression of iNOS and caspase-1 and upregulated IL-1Ra (M2). Moreover, $MGL1^-/CD11c^+$ eATMΦs upregulated transcripts involved in matrix remodeling and angiogenesis (ARG-1, ADAM-8, MMP-12, VEGF, and TGFβ-1). During the preparation of this manuscript, Fujisaka et al. (31) reported high levels of ARG-1 gene expression in $CD11c^+$ eATMΦs in mice fed an HFD for 17 weeks. Our results extend this observation and suggest that $MGL1^-/CD11c^+$ eATMΦs in the present study express a mixed M1/M2 remodeling phenotype.

Surprisingly, cluster-associated eATMΦs expressing both MGL1 and CD11c (i.e., $MGL1^{med}/CD11c^+$) constituted the majority (65–70%) of $CD11c^+$ eATMΦs (and ~50% of $CD11c^+$ eATMΦs after 20 weeks of HFD [not shown]). While this manuscript was in review, Westcott et al. (32) reported the unanticipated observation of substantially reduced numbers of $CD11c^+$ eATMΦs in $MGL1^{-/-}$ mice fed an HFD, thereby supporting our observation of the

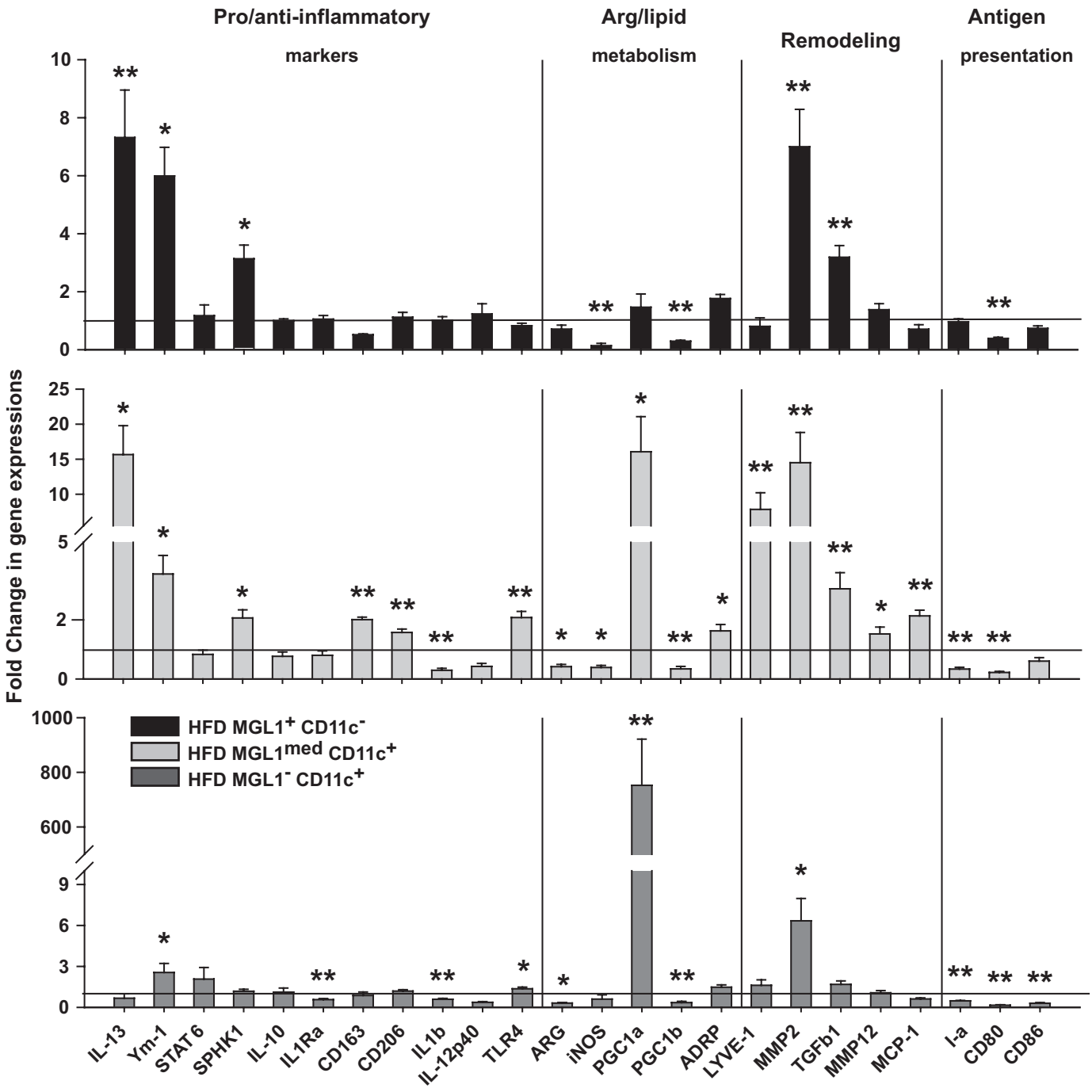


**FIG. 3. Prolonged (12-week) HFD feeding promotes M2-associated gene expression differentially in MGL1-expressing and CD11c-expressing eATMΦs. mRNA levels of inflammation-, metabolism-, remodeling-, and antigen presentation–related genes were analyzed by quantitative PCR after 12 weeks of HFD in each eATMΦ subtype (supplemental Fig. 3). mRNA levels were compared with levels determined after 8 weeks of HFD (set as "1" and indicated by the horizontal line). Data for each eATMΦ subtype are from 6 mice (week 8) and 9–11 mice (week 12), respectively. *$P < 0.05$; **$P < 0.01$, ANOVA and Tukey procedure.**

preponderance of MGL1-expressing CD11c$^+$ eATMΦs in the present study (Fig. 1). Occasional eATMΦs expressing both MGL1 and CD11c were previously identified next to clusters (11), but the phenotype of these eATMΦs was undetermined. MGL1$^{med}$/CD11c$^+$ eATMΦs express a mixed M1/M2 phenotype with transcript levels intermediate between MGL1$^+$/CD11c$^-$ and MGL1$^-$/CD11c$^+$ eATMΦs. This intermediate phenotype raised the possibility that MGL1$^{med}$/CD11c$^+$ eATMΦs were derived from interstitial MGL1$^+$/CD11c$^-$ cells. Lipid scavenging, a key function of eATMΦs in obesity (7), promotes CD11c expression in MΦs (33) and could conceivably promote the phenotypic progression of CD11c$^-$ eATMΦs to a CD11c$^+$ phenotype. However, the almost total absence of PKH26 dye among MGL1$^{med}$/CD11c$^+$ eATMΦs argues against their phenotypic progression from resident MGL1$^+$/CD11c$^-$ eATMΦs (Fig. 1*E*). Irrespective of origins, the phenotype of MGL1$^{med}$/CD11c$^+$ eATMΦs is likely to reflect exposure to two sets of adipose tissue microenvironmental cues (e.g., cytokines, lipid, and hypoxia) that individually elicit the discrete phenotypes of MGL1$^+$/CD11c$^-$ and MGL1$^-$/CD11c$^+$ eATMΦs, respectively.

TABLE 3
Fold difference in mRNA levels of genes regulating inflammation, metabolism, tissue remodeling, and antigen presentation in eATMΦ subtypes after 12 weeks of HFD relative to benchmark M2-polarized MGL1$^+$/CD11c$^-$ eATMΦs from mice fed an LFD for 8 weeks

| | 8 weeks LFD | 12 weeks HFD | | |
|---|---|---|---|---|
| | MGL1$^+$ CD11c$^-$ | MGL1$^+$ CD11c$^-$ | MGL1$^{med}$ CD11c$^+$ | MGL1$^-$ CD11c$^+$ |
| Pro-/anti- Inflammatory markers | | | | |
| Gene | | | | |
| IL-13 | * | 8.15 ± 3.09† | 2.08 ± 0.66* | 0.15 ± 0.11‡ |
| Ym-1 | * | 7.98 ± 2.16† | 1.04 ± 0.18* | 0.68 ± 0.17* |
| STAT6 | * | 5.24 ± 1.78† | 1.51 ± 0.25* | 0.86 ± 0.20* |
| SPHK1 | * | 0.52 ± 0.08† | 0.41 ± 0.05† | 0.22 ± 0.02‡ |
| IL-10 | * | 1.32 ± 0.11† | 0.62 ± 0.12‡ | 0.75 ± 0.20*‡ |
| IL-1Ra | * | 2.94 ± 0.35† | 8.47 ± 1.56‡ | 7.40 ± 1.01‡ |
| CD163 | * | 0.28 ± 0.01† | 0.13 ± 0.006‡ | 0.02 ± 0.005‡ |
| CD206 | * | 0.57 ± 0.12† | 0.38 ± 0.03† | 0.22 ± 0.02‡ |
| Clec-7a | * | 1.05 ± 0.18* | 1.36 ± 0.20*† | 1.84 ± 0.19† |
| IL-1β | * | 1.15 ± 0.12* | 0.95 ± 0.17* | 1.99 ± 0.21† |
| Caspase-1 | * | 0.57 ± 0.04* | 0.54 ± 0.05* | 0.52 ± 0.05* |
| IL-12p40 | * | 4.85 ± 1.24† | 6.80 ± 1.61† | 11.4 ± 3.53† |
| TLR-4 | * | 0.91 ± 0.09* | 0.89 ± 0.09* | 0.56 ± 0.05† |
| MCP-1 | * | 0.37 ± 0.10† | 0.21 ± 0.02† | 0.03 ± 0.004‡ |
| Metabolism | | | | |
| Genes | | | | |
| ARG-1 | * | 0.70 ± 0.13* | 0.93 ± 0.17* | 0.98 ± 0.12* |
| iNOS | * | 0.53 ± 0.25* | 0.09 ± 0.01† | 0.03 ± 0.01‡ |
| PGC-1α | * | 43.7 ± 13.6† | 283.4 ± 88.5‡ | 107.8 ± 24.2‡ |
| PGC-1β | * | 0.56 ± 0.07† | 0.56 ± 0.13† | 0.53 ± 0.14† |
| ADRP | * | 1.75 ± 0.14† | 2.26 ± 0.30† | 2.24 ± 0.26† |
| Remodeling | | | | |
| Genes | | | | |
| MMP-2 | * | 4.95 ± 0.91† | 6.39 ± 1.90† | 1.66 ± 0.48* |
| MMP-12 | * | 40.7 ± 10.3† | 360 ± 55‡ | 292 ± 46‡ |
| TGFβ-1 | * | 2.43 ± 0.35† | 2.36 ± 0.49† | 2.41 ± 0.42† |
| VEGF | * | 2.48 ± 0.17† | 5.48 ± 1.17‡ | 8.95 ± 2.53‡ |
| ADAM-8 | * | 6.18 ± 0.38† | 14.28 ± 0.82‡ | 14.57 ± 0.77‡ |
| LYVE-1 | * | 0.42 ± 0.15† | 0.26 ± 0.08† | 0.005 ± 0.001‡ |
| Antigen presentation | | | | |
| Genes | | | | |
| I-a | *‡ | 0.71 ± 0.08* | 0.46 ± 0.08† | 0.99 ± 0.07‡ |
| CD80 | * | 0.37 ± 0.04† | 0.26 ± 0.04‡ | 0.18 ± 0.04‡ |
| CD86 | * | 0.48 ± 0.05† | 0.17 ± 0.03‡ | 0.10 ± 0.02‡ |

Data are means ± SE. Means designated by different symbols are significantly different ($P < 0.05$, ANOVA and Tukey procedure).

Continued (12-week) HFD promoted M2-like transcriptional modulation in each of the three eATMΦ subtypes (Fig. 3). MGL1-expressing eATMΦs upregulated hallmark M2 genes and downregulated iNOS (Fig. 3). The MGL1$^{med}$/CD11c$^+$ subtype additionally upregulated MMP-2, CD163, and LYVE-1 (Fig. 3) and was three times more likely than other eATMΦ subtypes to stain for the IB4 isolectin (data not shown), a marker of adipogenic and angiogenic activities in eAT of obese mice (14). The increases in LYVE-1 and MMP-2 mRNAs are intriguing in light of proposed role of LYVE-1$^+$ eATMΦs in new vessel development during eAT expansion (19), and the demonstration that MMP-2 is required for diet-induced adipocyte hypertrophy (26). These observations are consistent with the localization of MGL1$^{med}$/CD11c$^+$ eATMΦs to remodeling clusters (Fig. 2) and suggest a functional role in angiogenesis and/or adipogenesis.

An unexpected feature of CD11c$^+$ eATMΦ gene expression at HFD week 12 was the robust upregulation of PGC-1α (Fig. 3) (rev. in 34). Although little is known concerning the role of PGC-1α in MΦ polarization (35), its role in promoting mitochondrial biogenesis and oxidative metabolism suggests that, similar to PGC-1β (28), PGC-1α–mediated gene expression promotes/maintains the M2 state. MGL1$^{med}$/CD11c$^+$ eATMΦs additionally expressed high levels of PPAR-α mRNA, suggesting increased fatty acid metabolism and blunted proinflammatory responses to Th1 cytokines (36). At HFD week 12, both CD11c$^+$ eATMΦ subtypes expressed reduced levels of M1-associated transcripts (iNOS, IL-1β, I-a, and CD80) as well as ARG-1 mRNA. These reductions suggest a relatively deactivated M2c phenotype, consistent with the elevated IL-10 gene expression observed in eAT at this time (Fig. 5) (12). Similar downregulation of M1 cytokines, iNOS and ARG-1 is observed in M2c-polarized MΦs during the reparative phase of murine muscular dystrophy (37).

Systemic PPAR-γ activation by thiazolidinediones (TZDs) promotes ATMΦ recruitment, M2-associated gene expression, and tissue remodeling in eAT of obese rodents (29,30,38,39). Surprisingly, acute (1-week) exposure to TZDs also increases CD11c mRNA in eAT (38) (Fig. 4). The seemingly anomalous observation of increased CD11c gene expression in response to M2-polarizing treatment is explained by our demonstration that MGL1$^{med}$/CD11c$^+$

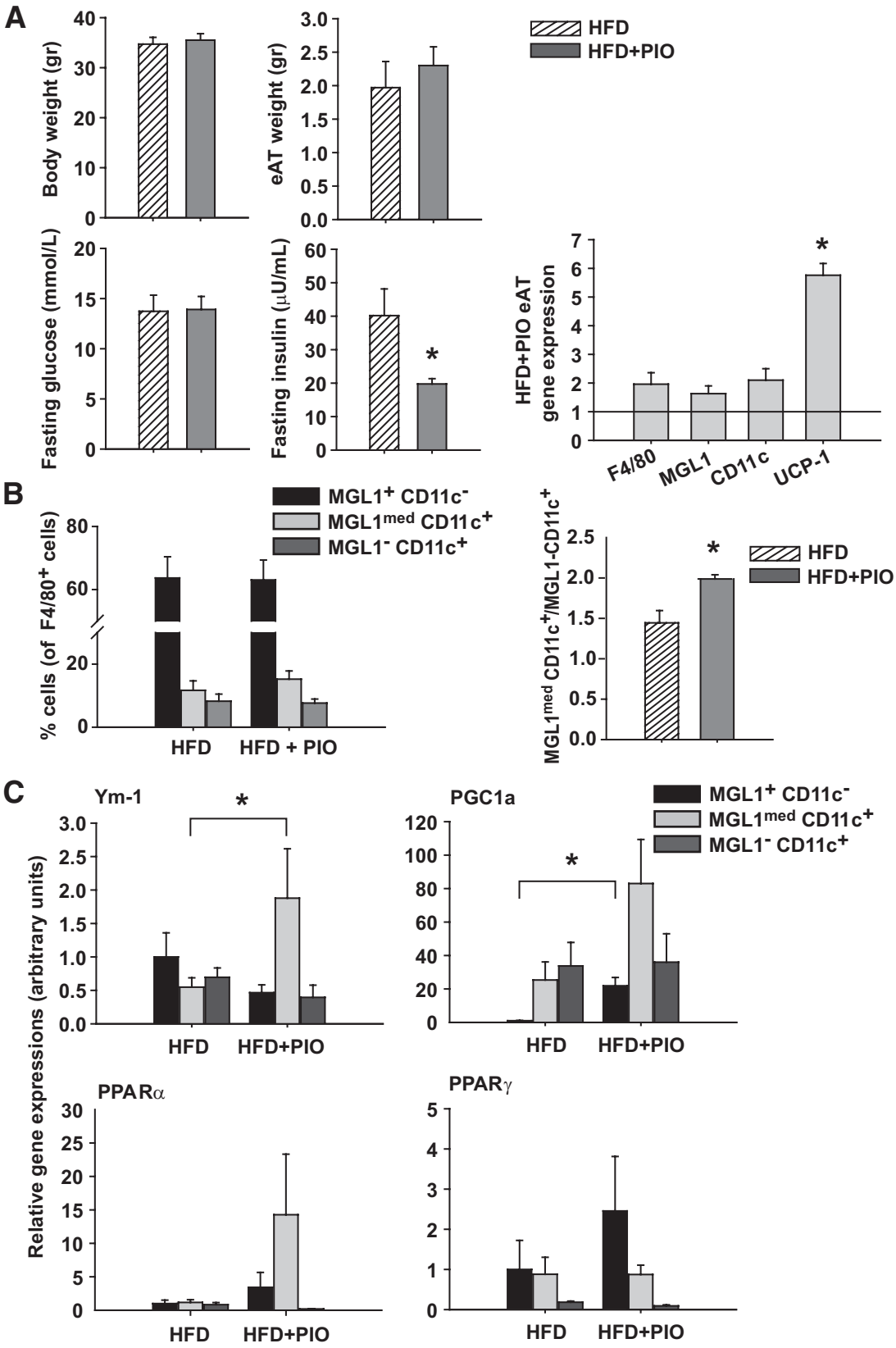


**FIG. 4. Pioglitazone treatment preferentially enhances accumulation of MGL1$^{med}$/CD11c$^{+}$ eATMΦs and promotes their expression of M2-associated genes. Mice fed an HFD for 10 weeks were fed an HFD or HFD containing PIO (0.01% [wt/wt]) (HFD+PIO) for 6 additional days. *A*: Body and eAT weights (*top panels*), fasting glucose and insulin levels (*bottom panels*), and gene expression relative to mice fed an HFD alone (*right panel*), $n = 4$. *B*: Flow-cytometric analysis of eAT indicating selective increase in MGL1$^{med}$/CD11c$^{+}$ eATMΦs (*left panel*) and enrichment in the proportion of CD11c$^{+}$cells expressing MGL1 (*right panel*), $n = 6$. *C*: Gene expression indicating a PIO-associated increase in Ym-1, PGC-1α, and PPAR-α transcripts in the MGL1$^{med}$/CD11c$^{+}$ subtype, $n = 6$. Similar patterns of gene expression were observed at HFD week 12 (Fig. 3 and supplemental Fig. 4). *$P < 0.05$, *t* test, or ANOVA with Tukey procedure.**

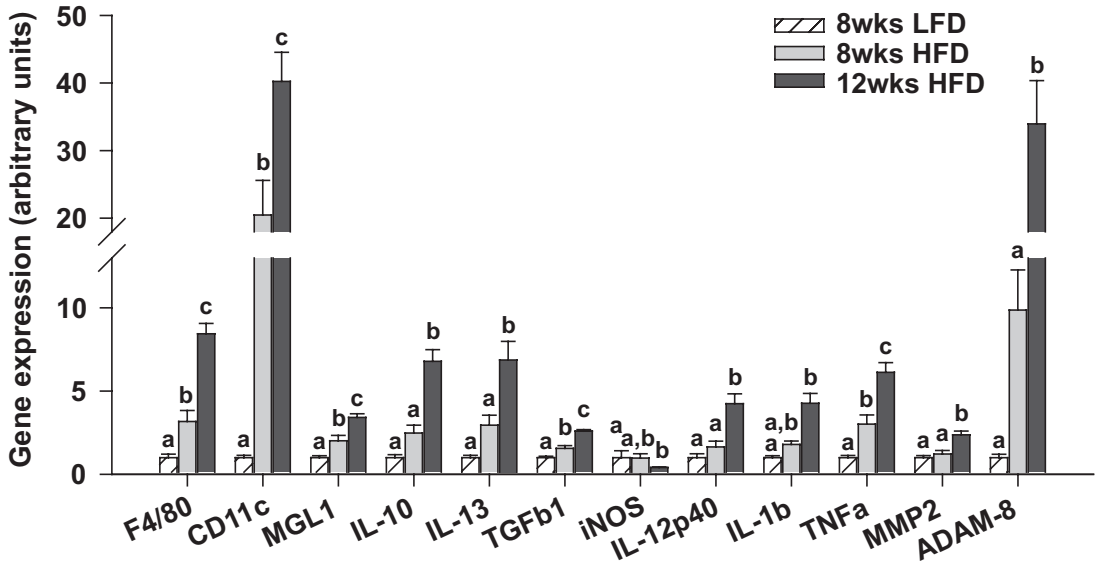


**FIG. 5. Coordinate expression of M1 and M2/remodeling genes in whole eAT during the HFD time course. Quantitative PCR was performed on eAT from mice fed the LFD (set as "1") or the HFD for either 8 or 12 weeks ($n$ = 6–8 mice per group). Means designated by different letters are significantly different ($P < 0.05$, ANOVA and Tukey procedure).**

eATMΦs selectively accumulate in eAT of obese mice fed the TZD PIO, a PPAR-γ/-α agonist (40). MGL1$^{med}$/CD11c$^{+}$ eATMΦs in mice fed HFD+PIO upregulated the M2-associated transcripts Ym-1, PGC-1α, and PPAR-α (Fig. 4) similar to MGL1$^{med}$/CD11c$^{+}$ eATMΦs in mice fed an HFD for 12 weeks (Fig. 3 and supplemental Fig. 4). These observations support the notion that MGL1$^{med}$/CD11c$^{+}$ eATMΦs become more M2 polarized at HFD week 12 and suggest that PPAR-γ (and/or PPAR-α) activation by endogenous ligands contributes to this polarization.

TZDs promote insulin sensitivity, in part, by promoting fat oxidation and the remodeling of adipose tissue with additional, small adipocytes (29,39,41,42). Our data suggest that these actions may be promoted in eAT with minimal inflammatory impact by the selective recruitment of MGL1$^{med}$/CD11c$^{+}$ eATMΦs expressing high levels of IL-13, PGC-1α, MMP-2, and LYVE-1 and relatively reduced levels of IL-1β and IL-12p40 as compared with MGL1$^{-}$/CD11c$^{+}$ eATMΦs (Table 3). However, the whole-body insulin-sensitizing effects of PIO also reflect its beneficial actions in multiple cells and tissues, including subcutaneous adipose tissue (39,41,42). Thus, despite increases in MGL1$^{med}$/CD11c$^{+}$ at HFD week 12, increased insulin resistance (Table 1) is not totally unexpected at this time given the coincident increase in MGL1$^{-}$/CD11c$^{+}$ eATMΦs (Fig. 1*D*) in the absence of the pleiotropic ameliorative actions of PIO.

In closing, we note that the mixed M1/M2 eATMΦ phenotypes described above were associated with progressively increasing and coordinate expression of M1 and M2/remodeling genes in whole eAT (Fig. 5). Multiple eAT cell types, in addition to eATMΦs, undoubtedly contribute to this mixed inflammatory profile. Nevertheless, our data demonstrate that HFD-induced whole-body insulin resistance (Table 1) develops in this model coincident with both an M2 as well as an M1 progression in eAT. This conclusion may reflect our use of a 60% (kcal) HFD, containing 33% more energy from fat than the diet used by Lumeng and colleagues (10,11) to elucidate the M1 eATMΦ switch. Although qualitatively identical, the higher fat content may promote more eAT remodeling and may coincidentally attenuate MΦ proinflammatory signaling (43). In particular, lipid scavenging by CD11c$^{+}$ eATMΦs at sites of adipocyte death (7) may render them particularly prone to the M1-inhibiting and/or M2-promoting effects of particular fatty acids (43,44). Future studies will address mechanisms by which dietary fat and/or adipose tissue microenvironments shape ATMΦ polarization and its inflammatory and metabolic sequelae.

## ACKNOWLEDGMENTS

This work was supported by National Institute of Health Grants DK074979 (to M.S.O.) and TH32HL69772 (to G.B.), American Diabetes Association Grants 1-06-RA-96 (to M.S.O.) and 7-08-RA-57 (to A.S.G.), Takeda Pharmaceuticals (to M.S.O.), and U.S. Department of Agriculture Contract no. 5819507707 (to A.S.G.).

No potential conflicts of interest relevant to this article were reported.

Parts of this article were presented at the Keystone Symposia, "The Macrophage: Intersection of Pathogenic and Protective Inflammation," Banff, Alberta, Canada, 12–17 February 2010.

We thank Allen Parmelee and Stephen Kwok from the Tufts University flow cytometry core facility for assistance.

## REFERENCES

1. Gutierrez DA, Puglisi MJ, Hasty AH. Impact of increased adipose tissue mass on inflammation, insulin resistance, and dyslipidemia. Curr Diab Rep 2009;9:26–32
2. Shoelson SE, Herrero L, Naaz A. Obesity, inflammation, and insulin resistance. Gastroenterology 2007;132:2169–2180
3. Weisberg SP, McCann D, Desai M, Rosenbaum M, Leibel RL, Ferrante AW Jr. Obesity is associated with macrophage accumulation in adipose tissue. J Clin Invest 2003;112:1796–1808
4. Odegaard JI, Chawla A. Mechanisms of macrophage activation in obesity-induced insulin resistance. Nat Clin Pract Endocrinol Metab 2008;4:619–626
5. Martinez FO, Helming L, Gordon S. Alternative activation of macrophages: an immunologic functional perspective. Annu Rev Immunol 2009;27:451–483

6. Martinez FO, Sica A, Mantovani A, Locati M. Macrophage activation and polarization. Front Biosci 2008;13:453–461
7. Cinti S, Mitchell G, Barbatelli G, Murano I, Ceresi E, Faloia E, Wang S, Fortier M, Greenberg AS, Obin MS. Adipocyte death defines macrophage localization and function in adipose tissue of obese mice and humans. J Lipid Res 2005;46:2347–2355
8. Mosser DM, Edwards JP. Exploring the full spectrum of macrophage activation. Nat Rev Immunol 2008;8:958–969
9. Ricardo SD, van Goor H, Eddy AA. Macrophage diversity in renal injury and repair. J Clin Invest 2008;118:3522–3530
10. Lumeng CN, Bodzin JL, Saltiel AR. Obesity induces a phenotypic switch in adipose tissue macrophage polarization. J Clin Invest 2007;117:175–184
11. Lumeng CN, DelProposto JB, Westcott DJ, Saltiel AR. Phenotypic switching of adipose tissue macrophages with obesity is generated by spatiotemporal differences in macrophage subtypes. Diabetes 2008;57:3239–3246
12. Strissel KJ, Stancheva Z, Miyoshi H, Perfield JW, 2nd, DeFuria J, Jick Z, Greenberg AS, Obin MS. Adipocyte death, adipose tissue remodeling, and obesity complications. Diabetes 2007;56:2910–2918
13. Lumeng CN, Deyoung SM, Bodzin JL, Saltiel AR. Increased inflammatory properties of adipose tissue macrophages recruited during diet-induced obesity. Diabetes 2007;56:16–23
14. Nishimura S, Manabe I, Nagasaki M, Hosoya Y, Yamashita H, Fujita H, Ohsugi M, Tobe K, Kadowaki T, Nagai R, Sugiura S. Adipogenesis in obesity requires close interplay between differentiating adipocytes, stromal cells, and blood vessels. Diabetes 2007;56:1517–1526
15. Pang C, Gao Z, Yin J, Zhang J, Jia W, Ye J. Macrophage infiltration into adipose tissue may promote angiogenesis for adipose tissue remodeling in obesity. Am J Physiol Endocrinol Metab 2008;295:E313–E322
16. Zeyda M, Stulnig TM. Adipose tissue macrophages. Immunol Lett 2007;112:61–67
17. Zeyda M, Farmer D, Todoric J, Aszmann O, Speiser M, Gyori G, Zlabinger GJ, Stulnig TM. Human adipose tissue macrophages are of an anti-inflammatory phenotype but capable of excessive pro-inflammatory mediator production. Int J Obes (Lond) 2007;31:1420–1428
18. Bourlier V, Zakaroff-Girard A, Miranville A, De Barros S, Maumus M, Sengenes C, Galitzky J, Lafontan M, Karpe F, Frayn KN, Bouloumie A. Remodeling phenotype of human subcutaneous adipose tissue macrophages. Circulation 2008;117:806–815
19. Cho CH, Koh YJ, Han J, Sung HK, Jong Lee H, Morisada T, Schwendener RA, Brekken RA, Kang G, Oike Y, Choi TS, Suda T, Yoo OJ, Koh GY. Angiogenic role of LYVE-1-positive macrophages in adipose tissue. Circ Res 2007;100:e47–57
20. Neels JG, Thinnes T, Loskutoff DJ. Angiogenesis in an in vivo model of adipose tissue development. FASEB J 2004;18:983–985
21. Greenberg AS, Egan JJ, Wek SA, Garty NB, Blanchette-Mackie EJ, Londos C. Perilipin, a major hormonally regulated adipocyte-specific phosphoprotein associated with the periphery of lipid storage droplets. J Biol Chem 1991;266:11341–11346
22. Chavey C, Mari B, Monthouel MN, Bonnafous S, Anglard P, Van Obberghen E, Tartare-Deckert S. Matrix metalloproteinases are differentially expressed in adipose tissue during obesity and modulate adipocyte differentiation. J Biol Chem 2003;278:11888–11896
23. Knolle MD, Owen CA. ADAM8: a new therapeutic target for asthma. Expert Opin Ther Targets 2009;13:523–540
24. Nguyen MT, Favelyukis S, Nguyen AK, Reichart D, Scott PA, Jenn A, Liu-Bryan R, Glass CK, Neels JG, Olefsky JM. A subpopulation of macrophages infiltrates hypertrophic adipose tissue and is activated by free fatty acids via toll-like receptors 2 and 4 and JNK-dependent pathways. J Biol Chem 2007;282:35279–35292
25. Ruan H, Zarnowski MJ, Cushman SW, Lodish HF. Standard isolation of primary adipose cells from mouse epididymal fat pads induces inflammatory mediators and down-regulates adipocyte genes. J Biol Chem 2003;278:47585–47593
26. Van Hul M, Lijnen HR. A functional role of gelatinase A in the development of nutritionally induced obesity in mice. J Thromb Haemost 2008;6:1198–1206
27. Niu J, Kolattukudy PE. Role of MCP-1 in cardiovascular disease: molecular mechanisms and clinical implications. Clin Sci (Lond) 2009;117:95–109
28. Vats D, Mukundan L, Odegaard JI, Zhang L, Smith KL, Morel CR, Wagner RA, Greaves DR, Murray PJ, Chawla A. Oxidative metabolism and PGC-1beta attenuate macrophage-mediated inflammation. Cell Metab 2006;4:13–24
29. Odegaard JI, Ricardo-Gonzalez RR, Goforth MH, Morel CR, Subramanian V, Mukundan L, Red Eagle A, Vats D, Brombacher F, Ferrante AW, Chawla A. Macrophage-specific PPARgamma controls alternative activation and improves insulin resistance. Nature 2007;447:1116–1120
30. Bassaganya-Riera J, Misyak S, Guri AJ, Hontecillas R. PPAR gamma is highly expressed in F4/80(hi) adipose tissue macrophages and dampens adipose-tissue inflammation. Cell Immunol 2009;258:138–146
31. Fujisaka S, Usui I, Bukhari A, Ikutani M, Oya T, Kanatani Y, Tsuneyama K, Nagai Y, Takatsu K, Urakaze M, Kobayashi M, Tobe K. Regulatory mechanisms for adipose tissue M1 and M2 macrophages in diet-induced obese mice. Diabetes 2009;58:2574–2582
32. Westcott DJ, Delproposto JB, Geletka LM, Wang T, Singer K, Saltiel AR, Lumeng CN. MGL1 promotes adipose tissue inflammation and insulin resistance by regulating 7/4hi monocytes in obesity. J Exp Med 2009;206:3143–3156
33. Cho HJ, Shashkin P, Gleissner CA, Dunson D, Jain N, Lee JK, Miller Y, Ley K. Induction of dendritic cell-like phenotype in macrophages during foam cell formation. Physiol Genomics 2007;29:149–160
34. Handschin C, Spiegelman BM. Peroxisome proliferator-activated receptor gamma coactivator 1 coactivators, energy homeostasis, and metabolism. Endocr Rev 2006;27:728–735
35. Sonoda J, Laganiere J, Mehl IR, Barish GD, Chong LW, Li X, Scheffler IE, Mock DC, Bataille AR, Robert F, Lee CH, Giguere V, Evans RM. Nuclear receptor ERR alpha and coactivator PGC-1 beta are effectors of IFN-gamma-induced host defense. Genes Dev 2007;21:1909–1920
36. Crisafulli C, Cuzzocrea S. The role of endogenous and exogenous ligands for the peroxisome proliferator-activated receptor alpha (PPAR-alpha) in the regulation of inflammation in macrophages. Shock 2009;32:62–73
37. Villalta SA, Nguyen HX, Deng B, Gotoh T, Tidball JG. Shifts in macrophage phenotypes and macrophage competition for arginine metabolism affect the severity of muscle pathology in muscular dystrophy. Hum Mol Genet 2009;18:482–496
38. Stienstra R, Duval C, Keshtkar S, van der Laak J, Kersten S, Muller M. Peroxisome proliferator-activated receptor gamma activation promotes infiltration of alternatively activated macrophages into adipose tissue. J Biol Chem 2008;283:22620–22627
39. de Souza CJ, Eckhardt M, Gagen K, Dong M, Chen W, Laurent D, Burkey BF. Effects of pioglitazone on adipose tissue remodeling within the setting of obesity and insulin resistance. Diabetes 2001;50:1863–1871
40. Orasanu G, Ziouzenkova O, Devchand PR, Nehra V, Hamdy O, Horton ES, Plutzky J. The peroxisome proliferator-activated receptor-gamma agonist pioglitazone represses inflammation in a peroxisome proliferator-activated receptor-alpha-dependent manner in vitro and in vivo in mice. J Am Coll Cardiol 2008;52:869–881
41. Coletta DK, Sriwijitkamol A, Wajcberg E, Tantiwong P, Li M, Prentki M, Madiraju M, Jenkinson CP, Cersosimo E, Musi N, Defronzo RA. Pioglitazone stimulates AMP-activated protein kinase signalling and increases the expression of genes involved in adiponectin signalling, mitochondrial function and fat oxidation in human skeletal muscle in vivo: a randomised trial. Diabetologia 2009;52:723–732
42. McLaughlin TM, Liu T, Yee G, Abbasi F, Lamendola C, Reaven G, Tsao P, Cushman S, Sherman A. Pioglitazone Increases the Proportion of Small Cells in Human Abdominal Subcutaneous Adipose Tissue. Obesity (Silver Spring), 2009
43. Zhou Q, Leeman SE, Amar S. Signaling mechanisms involved in altered function of macrophages from diet-induced obese mice affect immune responses. Proc Natl Acad Sci U S A 2009;106:10740–10745
44. Odegaard JI, Ricardo-Gonzalez RR, Red Eagle A, Vats D, Morel CR, Goforth MH, Subramanian V, Mukundan L, Ferrante AW, Chawla A. Alternative M2 activation of Kupffer cells by PPARdelta ameliorates obesity-induced insulin resistance. Cell Metab 2008;7:496–507